Understanding of the density profile shape, electron heat transport and internal transport barriers observed in ASDEX Upgrade

A.G. Peeters, C. Angioni, M. Apostoliceanu, G.V. Pereverzev, E. Quigley†, F. Ryter, D. Strintzi, F. Jenko, U. Fahrbach, C. Fuchs, O. Gehre, J. Hobirk, B. Kurzan, C.F. Maggi, A. Manini, P.J. McCarthy†, H. Meister, J. Schweinzer, J. Stober, W. Suttrop, G. Tardini, and the ASDEX Upgrade team.

Max-Planck-Institut für Plasmaphysik, EURATOM Association, D-85748 Garching
† University College Cork, Association Euratom-DCU, Cork, Ireland
e-mail: arp@ipp.mpg.de

Abstract In this paper several transport phenomena are described and explained through the properties of micro-instabilities. Linear and quasi-linear theory are used, which give a reasonable qualitative description of the relatively weak turbulent state of the plasma core. The paper deals with the following phenomena: density peaking, electron heat transport, density pump-out, reactor density profiles, stabilisation of the ion temperature gradient mode in transport barriers.

1. Collisionality dependence of particle transport

A clear dependence of density peaking on collisionality in H-mode plasmas has been observed on ASDEX Upgrade plasmas [1,2], and has recently been confirmed in experiments on JET [3]. The ASDEX Upgrade results are shown in Fig. 1, where the density at $\rho_{tor} = 0.4$ over the value at $\rho_{tor} = 0.8$ is plotted as a function of the collision frequency normalised to the drift frequency $\nu_{\rm eff} = \nu_{ei}/\omega_{DE} \approx 0.1 n_e Z_{eff} R/T_{ek}^2$, with n_e being the electron density in 10^{19} m^{-3}, and T_{ek} the electron temperature in keV.

Except for the lowest densities, H-mode plasmas are dominated by the ion temperature gradient mode (ITG). In low beta collisionless plasmas it is then mainly the non-adiabatic trapped electron response that can generate a particle flux. The electrons are collisionless in the sense that they perform many bounces in a collision time. However, the frequency (and growth rate) of the mode is not necessarily large compared with the de-trapping frequency of the trapped electrons. The comparison of the timescales is roughly expressed by $\nu_{\rm eff}$. For values of this parameter much larger than 1 the trapped particle response is strongly reduced on the timescale on which the mode grows, leading to a strongly reduced particle flux. This, in itself, does not explain the change in the peaking of the density profile, but indicates that the collisionality is a key parameter. It does, however, directly explain the observation that density profiles need more time to adjust at higher densities (higher collisionality).

To gain insight into the physics of particle transport we will first investigate the different possible contributions to the particle flux in a collisionless model. A generic model containing the electron continuity and energy balance equation yields for the particle flux (Γ) [5]

$$\Gamma = -\frac{f_t D_{ql}}{R}\left[\frac{R}{L_n} + C_T \frac{R}{L_{Te}} + 2 f_{De}(\hat{s}, q, \alpha, \ldots) C_q \frac{|R\nabla B|}{B}\right], \qquad (1)$$

where f_t is the trapped particle fraction, D_{ql} is the quasi-linear diffusion coefficient, and C_T $C_q = 1 + 2C_T/3$ are two parameters that depend on the mode frequency and growth rate. The particle flux consists of three contributions: A diagonal term (R/L_n) which represents the particle diffusion. A thermodiffusive term (R/L_{Te}) and a term related to the curvature of the magnetic field $R\nabla B/B$. In all the cases discussed in this paper the particle source plays a minor role in the determination of the density profile. The density gradient is, therefore, determined by the condition of approximately zero flux ($\Gamma \approx 0$), and it follows from the equation above that

$$\frac{R}{L_n} = -C_T \frac{R}{L_{Te}} - 2 f_{De}(\hat{s}, q, \alpha, \ldots) C_q \frac{|R\nabla B|}{B}, \qquad (2)$$

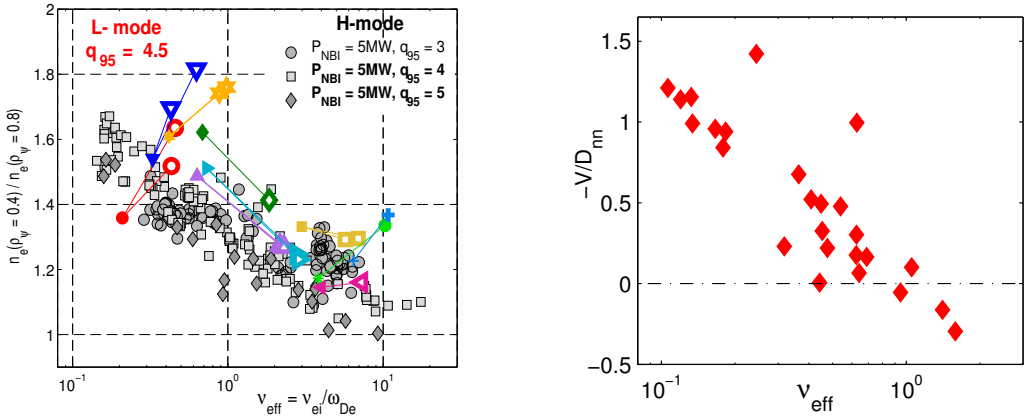

Figure 1: Left: Density peaking from DCN interferometer as a function of the normalised collisionality. Grey symbols are H-mode discharges, open coloured symbols are Ohmic discharges, and closed coloured symbols are L-mode ECH heated discharges. Right: The ratio of the pinch velocity and diffusion coefficient V/D of the GLF23 model as a function of the collisionality

i.e. the equilibrium density gradient is independent of the quasi-linear diffusion coefficient. In the description above, however, one has to keep in mind that an unstable mode does not exist in the whole parameter space (i.e. there is a second trivial solution to $\Gamma = 0$ namely $D_{ql} = 0$). A net inward particle flux due to the curvature pinch does not exist, because the mode would be stable in the corresponding region of parameter space. The electron temperature gradient, however, can generate a net inward flux.

The generic model descibed above is a subset of the gyrofluid model GLF23 [4]. The latter model contains the physics of the ITG and trapped electron mode (TEM) system as well as the dissipative effects introduced by collisions on the mentioned instabilities. It predicts [5] that the particle flux decreases with increasing collisionality as expected from the physical picture sketched above. The off-diagonal terms that are directed inward, i.e. the pinch velocity, however, decrease more strongly than the particle diffusion, as is shown in Fig. 1. This leads at higher density (and collisionality) to flater density profiles. By modifying the model, taking out the collisional effects, it has been checked that the above mentioned effects are indeed directly related to the collisions.

2. Electron heat transport

Electron heat transport under dominant electron heating has been extensively studied in ASDEX Upgrade [6–8], using electron cyclotron resonant heating (ECRH). These studies have (among others) lead to the following results: the electron heat flux is a non-linear function of the electron temperature gradient. There is evidence for a threshold in the electron temperature gradient below which the electron heat transport (nearly) vanishes. The profiles with central heating at different heating powers are resilient against profile changes. This resilence is, however, not absolute. Off-axis heating allowing for a large reduction of the heat flux in the confinement region, does lead to profile changes as can be seen in Fig. 2.

The electron heat transport has been investigated using the gyro-kinetic stability code GS2 [9]. This study [10] has enabled the explanation of many of the features described above. It has been found that the dominant micro-instability for low line averaged density ($n_{lin} \leq 3\ 10^{19}$ m^{-3}) is the trapped electron mode (TEM). The ion temperature gradient mode (ITG) can be unstable as well, but has generally a lower growth rate. The electron temperature gradient (ETG) mode, however is stable due to the large electron to ion temperature ratio.

The sensitivity of electron heat transport on plasma parameters has been studied with GS2

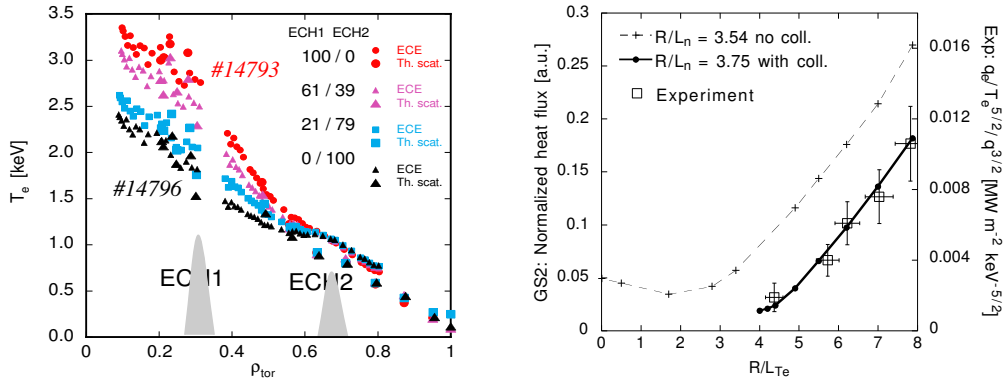

Figure 2: Left: Electron temperature profiles of a series of discharges in which the central heat flux was varied, without changing the heat flux through the edge. Right: Comparison of the normalized experimental heat flux with the GS2 calculations

through the variation of these parameters around a standard set which is directly obtained from one of the discharges. The threshold in $R/L_{Te} = R\nabla T_e/T_e$ of the TEM, as well as the heat flux at larger $R\nabla T_e/T_e$ is sensitive to the density gradient, collisions as well as the magnetic shear. The density gradient contributes strongly to the drive of the mode, and at a sufficiently large density gradient the mode is unstable for all temperature gradients. The magnetic shear stabilizes the mode both a high positive as well as at negative shear. The growth rate at the poloidal wave number where it has its maximum, is less sensitive to the safety factor, and ion temperature.
Figure 2 shows a set of experiments in which the heat flux in the core region was varied, without changing the heat flux in the outer region [8]. This has been done by switching the ECRH power from on to off-axis, while keeping the total power constant. These experiments aimed at the investigation of the heat flux as a function of the electron temperature gradient, with minimal changes to the electron temperature itself. The latter would have a strong influence through the gyro-Bohm factor. Also shown is a comparison of the normalized electron heat flux (eliminating the gyro-Bohm factor and safety factor dependence) with the quasi-linear calculations of the GS2 code. One free parameter, the saturation level, is adjusted here, and the heat flux has been calculated for the poloidal wave vector for which the growth rate is maximum. The plasma parameters used in the stability calculations are $T_e = 1.5$ keV, $n_e = 2.16 \cdot 10^{19}$ m^{-3}, $R/L_n = 3.5$, $T_i = 0.5$ keV, $R/L_{Ti} = 0$, $\varepsilon = 0.177$, $\hat{s} = 1$, $q = 1.57$, and are all, as well as possible, taken from the experiment [10]. (The determination of the ion temperature has error bars of typicall 20 % and, therefore, its gradient has been set to zero). The dashed line gives the code result without collisions. No threshold exists for this case, and no good agreement with the experiment can be obtained, i.e. collisions ($\nu_{\text{eff}} \approx 0.25$ here) are an important ingredient for the quantitative description of the transport even a low densities. The thick curve shows the results with collisions, and with a slightly higher density gradient $R/L_n = 3.75$ compared to the measured value $R/L_n = 3.5$, with the difference, however, being well inside the error bars which are typically 20% . It can be seen that good agreement between the calculations and the experimental results is obtained.
This figure visualizes many of the previously mentioned observations. The heat flux is not linear in the gradient. The apparent threshold (obtained through extrapolating the heat flux as a function of the gradient towards zero) agrees well with the simulations. The results also describe a moderately stiff situation, i.e. the threshold can be exceeded by a factor 2 for the highest ECRH heat flux. The maximum electron cyclotron heating power is 2MW in ASDEX Upgrde. Neutral beams could give a much higher heat flux (20 MW power installed), but of

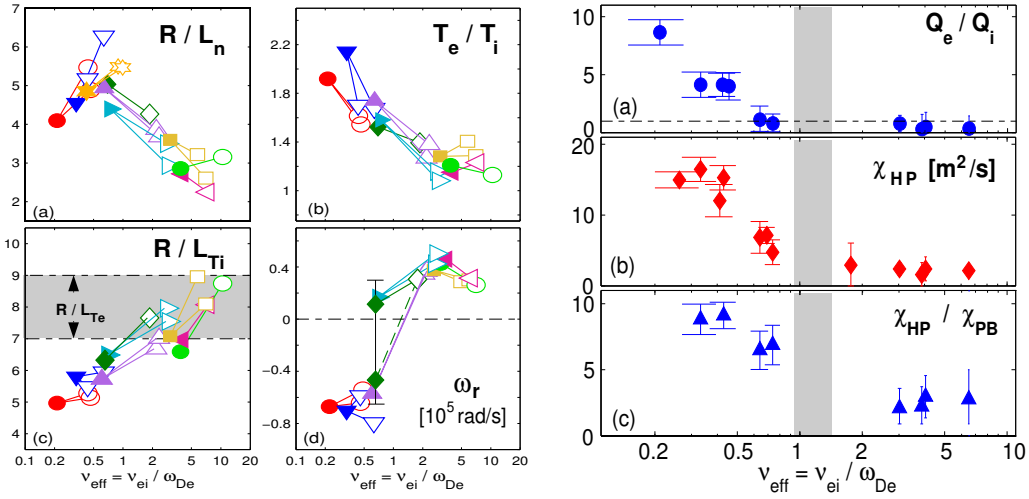

Figure 3: Left: gradient lengths of the relevant profiles as well as electron to ion temperature ratio and the frequency of the most unstable mode as a function of normalized collsionality. Right: electron to ion heat flux ration and heat pulse conductivities

course would heat the ions as well.

All of the above results refer to low density plasmas, or more accurately low collisionality plasmas. If the density is raised, collisionality increases and the TEM becomes weaker. This leads eventually to a transition in which the dominant mode becomes an ITG ($n_{lin} \approx 3.5 \cdot 10^{19}$ m^{-3}), and at even higher density to a complete stabilization of the TEM ($n_{lin} \approx 6 \cdot 10^{19}$ m^{-3}). The ITG transports both ion as well as electron heat, but the latter is smaller than the former. The transition to a dominant ITG is, therefore, also closely connected with the collisional energy coupling of the channels, increasing the ion heat flux, and controlling the transition over the gradients and temperature ratio. Since the ITG is dominantly driven by the ion temperature gradient, the electron heat flux becomes a weak function of the electron temperature gradient. The heat conductivity coefficient as determined from the heat wave $\chi_{HP} = \partial q_e / \partial n \nabla T$) decreases strongly compared with the power balance χ_{PB} value. This behaviour is shown in figure 3. Intrestingly, the transition from a dominant TEM to a dominant ITG, as indicated by the shaded region in the right graph, coincides with the transition from the Linear Ohmic Confinement regime to the Saturated Ohmic Confinement regime.

3. Density pump out

An important phenomenon in the determination of the density profile shape is the so-called pumpout. This refers to an observed flattening when heating (mostly electron heating) is applied. Investigations on ASDEX Upgrade [5] have, however, shown that this is not a universal phenomenon. In H-mode plasmas flattening occurs at low density $n_{lin} \approx 4 \cdot 10^{19}$ m^{-3} as well as at densities close to the Greenwald limit, with the profile showing a small peaking at the intermediate densities. A similar behaviour is observed in L-mode plasmas, as shown in Fig. 1 by the coloured symbols. The lines connecting these symbols show the change in peaking when going from the Ohmic (open symbol) to the ECH heated phase (closed symbol).

Again this observation can be explained by the behaviour of the ITG/TEM system. The explanation is through the thermo-diffusive pinch in the particle flux. Many experiments have reported that there is no evidence for such a term, but it must be noted that R/L_{Te} as well as C_T can be weakly varying with plasma parameters for a large part of the parameter space, making the effect difficult to observe. It was, however, shown [5] that the thermo-diffusion coefficient C_T changes sign (from inward to outward) if the mode rotation changes from the ion diamagnetic

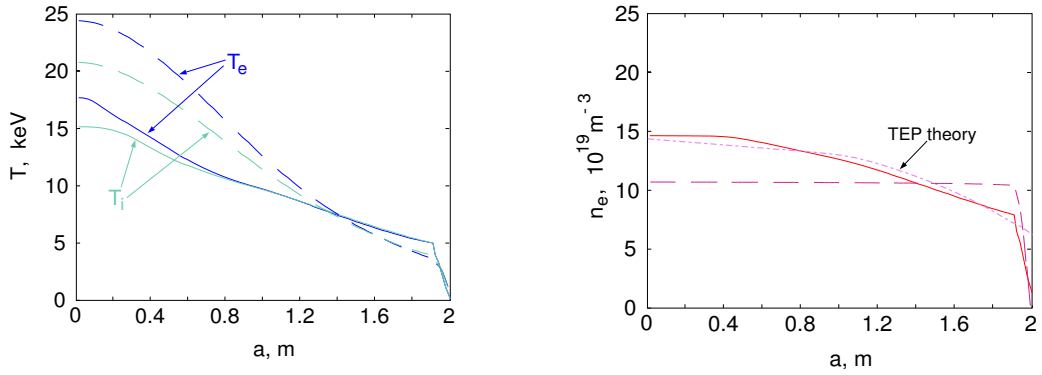

Figure 4: Steady state distributions of the plasma density n_e, electron T_e and ion T_i temperatures in ITER as functions of the minor radius a in the mid-plane. Full curves show the results of the GLF23 model with the boundary conditions $n_{e,ped} = 7.9 \times 10^{20}$ m^{-3} and $T_{e,ped} = T_{i,ped} = 5$ keV at the pedestal top. Results of the scaling-based model [14] are shown with the broken lines. The dotted line shows prediction of the TEP theory where the shear profile is defined by the GLF23 modelling.

(ITG) to the electron diamagnetic direction (the direction of the TEM). Linear GS2 simulations of the L-mode discharges, shown in Fig. 2 (diagram with the mode frequency ω_r), confirm that the cases with density profile flattening have indeed the TEM as dominant instability, whereas at higher density the dominant mode is an ITG and, consistently, no flattening occurs. In the low density region the application of RF electron heating leads to a much larger electron temperature, and consequently a larger (negative) frequency of the mode. The thermodynamic outward pinch increases, leading to a profile flattening. Note from the right panel of figure 3 that in the low density region the ratio of heat pulse to power balance conductivity is high, whereas it is reduced in the higher density region, consistent with the GS2 calculations of a dominant TEM in the first and a dominant ITG in the latter region. The similar observation in H-mode at low density is explained in the same way. Here, a transition to dominant TEMs is generated at low density through the lower collisionality, as well as the larger density gradient, which gives more drive to the TEM. Again density pump-out is observed in the dominant TEM parameter region. In the L-mode discharges with line averaged densities around 3.5 10^{19} m^{-3} both TEM and ITG are equally strong. In this region the thermo-diffusion is expected to be very small [5,11]. The application of ECRH leads to a density peaking, which is consistent with a collisionality decrease generated by the higher electron temperature. This is the first evidence that the collisionality dependence of the density peaking plays a role in the L-mode as well.

4. Density profiles in a reactor

The studies presented in this paper have a strong impact on the expected density profile in a reactor. Current experiments at the density limit have a flat density profile which, in the lack of adequate models for prediction, is a reason to assume that this will also be the case for a reactor [13]. However, current experiments at the density limit have a high normalised collisionality, whereas this value is low in a reactor close to the density limit. From the collisionality dependence of the density peaking in H-mode discharges one expects, therefore, a more peaked profile than in present experiments at the density limit. There is a difference with current experiments also through the heated channel. The alpha particle heating in a reactor is mostly electron heating, and can lead to density pump out. The studies of the previous section, however, show that this pump out can only be expected when the dominant mode is a TEM. At low collisionalities a sufficient large density gradient is necessary for the TEM to dominate and, consequently,

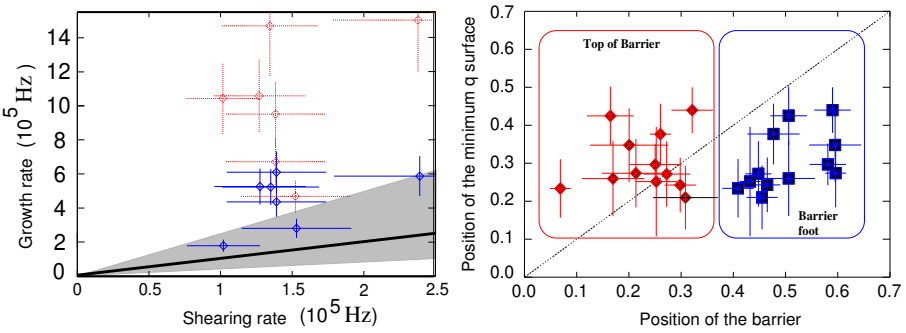

Figure 5: Left: Comparison of the growth rate of the most unstable mode with the shearing rate. Right: Position of the barrier top and foot compared with the minimum q position

a finite peaking can be expected.
Simulations for ITER parameters have been performed with the GLF23 model [14], with the results shown in Fig. 4. Here the volume averaged density $\langle n_e \rangle = 10^{20}$ m^{-3} is 80% of the Greenwald density and a edge pedestal temperature of 5 keV has been used to obtain an energy multiplication factor $Q = 10$, with 40 MW of NBI heating. Shown are the results of the GLF23 model (red line) together with the standard assumption (dashed line) as well as the result of the Turbulent Equipartition theory (pink line). The peaking of the density can be calculated to lead to an increase of 30% in the energy multiplication factor compared with the flat profile, for the same volume averaged density and ion temperature profile.
Analysing the growth rates of the modes it turns out that the working point is in the region in which the TEM and ITG are roughly equally strong. The thermo-diffusion is, therefore, expected to be small, and the density gradient determined by the curvature pinch. In this case very good agreement with the TEP [15,16] theory is obtained.

5. Stabilisation of the ITG in transport barriers

Further theoretical as well as experimental work has clarified several points in the stabilisation of the ITG in ion temperature transport barriers in ASDEX Upgrade. The standard paradigm that the shearing rate ($\omega_{E\times B}$) should exceed the growth rate (γ) of the most unstable mode can, so far, not be established, as shown in Fig. 5 [18] which compares the shearing rate with the growth rate, calculated without (red) and with (blue) the Shafranov shift. On the thick black line the criterion is satisfied. The grey area shows the quoted uncertainty of a factor 2.5 in the criterion [17], but there exist barriers for which $\gamma = 4\omega_{E\times B}$. The growth rates are again calculated using GS2, and the shearing rate is obtained from the toroidal rotation only (the neoclassical poloidal rotation does not largely change the result). The figure on the right of Fig. 5 also shows the position of the barrier top and foot compared with the position of the minimum q surface. Barriers have a tendency to span over the zero shear region, although there are barriers that lie entirely in the region of positive shear.
In order to resolve the discrepancy two non-standard mechanisms, which could change the growth rates of the modes have been investigated: the uniform electric field and zero magnetic shear.
Previously, it has been reported that a uniform electric field can stabilise the ITG in ASDEX Upgrade [19]. The mechanism through which this occurs is the poloidal rotation of the mode due to the $E \times B$ velocity, moving it in the favourable curvature region in which the mode is stable. It has now been found [20] that the background distribution used for this stability calculations plays an important role. A proper background, which is a solution of the gyro-kinetic equation has been constructed, and is shown to have a freedom in the choice of the

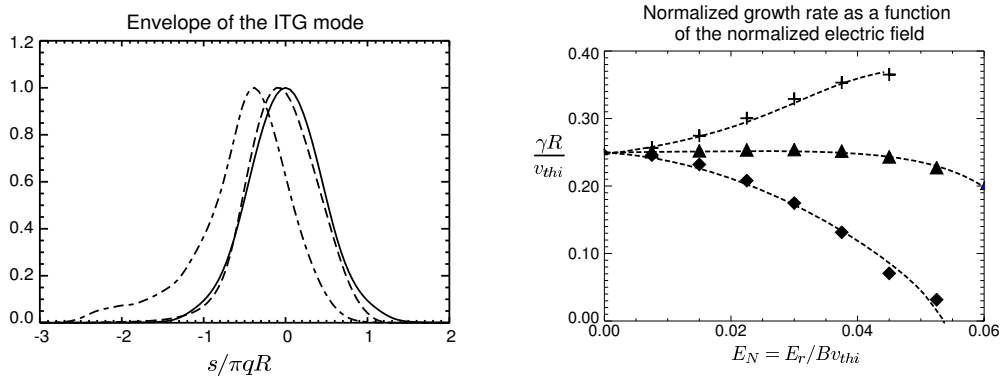

Figure 6: Left: Envelope of the absolute value of the potential of the ITG mode as a function of the field line length, without electric field (thick line), with an electric field but without toroidal rotation (dash-dot), and with an electric field entirely connected with a toroidal rotation (dashed) Right: Growth rate as a function of the electric field with (crosses) and without (diamonds) toroidal rotation

toroidal rotation at a given radial electric field, while always satisfying the radial force balance. The stabilisation occurs only when the toroidal rotation is small, while it is absent in the case with toroidal rotation.

This is shown in figure 6 which shows the mode structure for a certain value of the electric field, with and without rotation, as well as the growth rate as a function of the electric field (again with and without toroidal rotation). The parameters in this calculations are $q = 1$, $\hat{s} = 0.75$, $R/L_N = 2$, $R/L_T = 7$, $\varepsilon = 0.1$, $k_\theta \rho = 0.5$. (Note that the thermal velocity here is $v_{thi} = \sqrt{2T_i/m_i}$). It can be seen that with an electric field and zero toroidal rotation the mode is indeed rotated in the poloidal direction, and is more stable. However, when the poloidal plasma rotation is zero, and the electric field is entirely connected with the toroidal rotation, there is no stabilising effect. This means that the stabilisation by a uniform radial electric field does not play a large role in the experiment, since the electric field is found to be dominantly connected with a toroidal rotation.

A second possible mechanism is a strong stabilisation at zero shear (The ballooning transform used in GS2 and many other stability calculations can not be used for this case). On this subject several contradicting results have been published. The role of zero shear has been investigated using a newly developed global (simple torus) linear ITG code [21]. The global simulations show that zero shear does not lead to strong stabilisation despite the absence of resonant modes. The coupling between different poloidal modes is stronger than the damping due to the fact that they are non-resonant. This allows for the formation of a global mode with a ballooning structure, and a growth rate almost equivalent to the one with finite shear.

Both the uniform electric field as well as the zero magnetic shear, therefore, fail to explain the discrepancy between the shearing and growth rates. Three speculations on mechanisms that could do so are currently favoured: 1. There is a significant amount of non-thermal ions that leads to a stabilisation of the modes [22], 2. The pressure gradient of non-thermal ions, currently not included in the Shafranov shift calculation leads to further stabilisation (note that the Shafranov shift has a large impact in Fig. 5, 3. the barriers with the high growth rates are generally very narrow. Global effects (second derivatives of the profiles) could play a role.

Acknowledgements: We thank W. Dorland and M. Kotschenreuther for providing GS2, R. Waltz and J. Kinsley for GLF23, J. Weiland for the Weiland model.

References

[1] C. Angioni et al., Phys. Rev. Lett. (2003)**90**, 205003.

[2] C. Angioni et al., Phys. Plasma (2003) **10** 3225.

[3] H. Weisen, to be submitted to Nuclear Fusion (2004).

[4] R.E. Waltz et al., Phys. Plasmas (1997) **4**, 2482.

[5] C. Angioni et al., Nucl. Fusion (2004) **44**, 827.

[6] F. Ryter et al., Plasma Phys. Contr. Fusion (2001) **43** A323.

[7] G. Tardini et al., Nucl. Fusion (2002)**42** 258.

[8] F. Ryter et al., Nucl. Fusion (2003) **43** 1396.

[9] M. Kotschenreuther, G. Rewoldt, W.M. Tang, Comp. Phys. Comm. (1995) **88** 128.

[10] A.G. Peeters at al., submitted to Phys. of Plasmas

[11] X. Garbet et al., Phys. Rev. Lett. (2003) **91** 035001/

[12] C. Angioni et al., in preparation

[13] ITER final design report (2001), PDD, section 4, IAEA, Vienna, 2002 (http://www/naka.jaeri.jp/ITER/FDR/PDD).

[14] G.V. Pereverzev et al., submitted to Nucl. Fusion

[15] V.V. Yankov, JETP Lett. (1994) **60** 171.

[16] M.B. Isichenko et al., Phys. Rev. Lett. (1996) **64** 4436.

[17] Waltz R E, Kerbel G D, Milovich J and Hammett G W (1995) Phys. Plasmas (1995)**2** 2408.

[18] E. Quigley et al., accepted for publication in Nuclear Fusion.

[19] M. Maccio, J. Vaclavik, L. Villard, Phys. Plasmas (2001) **8**, 895.

[20] A. G. Peeters et al., Phys. of Plasmas (2004) **11** 3748.

[21] D. Strintzi et al., To be submitted to Phys. of Plasmas

[22] G. Tardini et al., 31th European Physical Society Conference on Controlled Fusion and Plasma physics (London 2004),